May 1986 LRP 290/86

COMPUTING OF RF HEATING AND CURRENT-DRIVE IN TOKAMAKS

K. Appert, T. Hellsten, O. Sauter, S. Succi,
J. Vaclavik and L. Villard

Invited Paper presented at

8th EPS Conf. on Computational Physics - Computing in Plasma Physics

Eibsee, near Garmisch-Partenkirchen, F.R. Germany

May 13 to 16, 1986

COMPUTING OF RF HEATING AND CURRENT-DRIVE IN TOKAMAKS

K. Appert, T. Hellsten*, O. Sauter, S. Succi,

J. Vaclavik and L. Villard

Centre de Recherches en Physique des Plasmas

Association Euratom - Confédération Suisse

Ecole Polytechnique Fédérale de Lausanne

21, Av. des Bains, CH-1007 Lausanne / Switzerland

* JET Joint Undertaking, Abingdon, OX14 3EA, Great Britain

Abstract

Two of the technically most developed numerical descriptions of radio frequency waves are discussed:Global-wave and quasilinear codes. The numerical approaches are presented within the physical context. The techniques considered are different finite element methods ranging from cubic Hermite finite elements to the non-conforming "finite hybrid elements". A high efficiency of the latter technique is demonstrated. The applications include Ion-Cyclotron Range of Frequency (ICRF) mode-conversion heating in JET, Alfvén Wave Range of Frequency (AWRF) and ICRF Heating in TCV, and runaway production in Lower-Hybrid Range of Frequency (LHRF) ramp-up.

1. Introduction

In the last decade a considerable number of new numerical tools have been developed for the study of RF heating and current drive. Concise reviews [1], and specialized research papers [2] in different areas of activity have been presented at the 3rd European Workshop on Problems in the Numerical Modeling of Plasmas (NUMOP) in Varenna last year. In the present report it could be attempted to review the reviews presented at the workshop. The outcoming enumeration, we are sure, would not be particularly zestful. In place, we intend to confront the reader with the merits and the limitations of our own numerical models. The general interest in this contribution is, however, preserved by the fact that these models appertain to those two areas of sophisticated RF numerics which presently are the most developed: the solution of linear global wave equations in plasma cavities (as opposed to ray tracing approaches) and the time evolution of particle distribution functions according to Fokker-Planck or quasilinear equations. Both areas are rapidly evolving under the stimulus of experimental results which show evidence for the excitation of eigenmodes in the ion-cyclotron range of frequency [3] (ICRF) and for the modification of the electron distribution function under the influence of waves in the lower hybrid range of frequency [4] (LHRF).

The plan of the paper is as follows. In Chapter 2 we present the computation of a mode conversion scenario in JET performed with our two-dimensional cold plasma code LION [5]. Playing the Devil's advocate we shall ask whether the result is at all credible and whether

the method used is the best. Using one- and two-dimensional cold and one-dimensional hot plasma models we shall document the difficulties in treating an ICRF scenario which is dominated by eigenmodes. In Chapter 3 we then pose similar questions concerning our new two-dimensional quasilinear code, ADLER [6]. In contrast to a Fokker-Planck code, a quasilinear code computes the self-consistent evolution of the wave spectral energy together with that of the particle distribution. Such a code is needed if eventually we want to model certain kinetic instabilities observed in some low-density discharges with and without LHRF current drive [7,8]. Again, the situations we have in mind are hard to treat numerically, a fact which obliges us to discuss the numerical methods in detail. Finally, in Chapter 4 we use our numerical tools to answer a few additional physical questions in different frequency domains.

2. Excitation of Global Waves in Bounded Plasmas

2.1 Physical background

Until recently the most common numerical approach to the excitation and propagation of waves in the range between the ion and electron cyclotron frequencies has been ray tracing based on the WKB approximation [9]. In the Alfvén Wave Range of Frequency (AWRF) this approach is manifestly impractical due to the fact that the wavelengths of the excited waves are of the order of the gradient scale lengths (minor radius of the torus). This is particularly true for the main AWRF heating scenario where the first radial eigenmode of the

fast magnetosonic wave is excited by antennae situated in the vacuum region between the plasma and the conducting wall [10]. In the WKB picture this mode is evanescent over the whole plasma minor radius.

With respect to the ICRF, in large devices like JET, originally it was felt that ray tracing should be appropriate because the wavelengths of the excited fast magnetosonic waves are small compared to the minor radius. Ray tracing is indeed appropriate in heating scenarii where most of the wave energy emitted by the antennae is absorbed over a few wavelengths. In this case no energy is reflected to the antenna, and the antenna does not feel any back EMF (electromotive force), or, in other words, the antenna does not excite any eigenmode of the plasma cavity. In the opposite case ray tracing, at least in its present form, is not applicable.

The alternative approach has become known as the "global-wave approach" implying that the solution of the pertinent wave equation contains incident and reflected waves, or, in other words, that the wave equation in the plasma is solved together with the wave equation in the vacuum and appropriate boundary and matching conditions at the interfaces plasma-vacuum, vacuum-antenna-vacuum and at the conducting wall.

The wave equation has the general form

$$\mathrm{rot}\,\mathrm{rot}\,\vec{E} = \frac{\omega^2}{c^2}\,\vec{\vec{\epsilon}}\cdot\vec{E} \qquad (1)$$

where $\vec{E}$, ω and c are the wave electric field, the applied frequency and the velocity of light, respectively. The dielectric tensor, $\overleftrightarrow{\epsilon}$, can have the most different forms depending on the plasma model used. It is a simple tensor in cold plasma theory [11] including low-β current-less MHD and is a spatial operator when equilibrium-current [5,12] or finite-temperature (finite larmor radius) effects [13] are included. In the case of low-frequency excitation ($\omega << \omega_{LH}$, lower hybrid frequency) use is made sometimes of the fact that $\epsilon_{zz} \to \infty$ as $m_e / m_i \to 0$, and $E_z \to 0$ as a consequence.

In all the models we have presented so far we have used the fact that $m_e << m_i$. This approach is mandatory in a cold plasma model in two dimensions [5] because it excludes small spatial scales which would be, as we shall see, difficult to resolve. In one dimension, however, where it is easy to solve even the wave equation of the hot plasma model [14] (for a review including 2D see [15]) and where small scales are already present due to the finite temperature effects, the approximation $m_e / m_i \to 0$ seems to be an unnecessary limitation of the computational model. Taking into account finite values of E_z turns eq. (1) from a 4th order into a 6th order ordinary differential equation (ODE) [15] which, from a numerical point of view, is an unsignificant complication. Physicswise an apparent advantage of this more complete model is the possibility of treating Landau damping consistently. Based on a general form of the dielectric tensor [16], we have recently developed a new version of the 1-D code ISMENE [14] applicable to any frequency domain.

In the course of this investigation we extensively use the 2D code LION described in Ref. 5, and compare the results with those obtained with the old version of ISMENE [14] applied to the hot and then to the cold plasma model which, in fact, turns eq. (1) into a 2nd order ODE. The new version of ISMENE, mentioned in the preceeding paragraph, has been used for one illustration only (Fig. 5).

2.2 ICRF heating in JET

The 2D code LION [5] permits the study of ICRF wave propagation in a low-β plasma confined in an axisymmetric torus. It uses the same geometry, spatial operators and equilibria as the ideal-MHD stability code ERATO [17]. It is based on the cold plasma model and, hence, the waves are absorbed merely by resonance absorption as in the AWRF case [12,18]. It is a trivial matter to add ion-cyclotron absorption to the cold $\overleftrightarrow{\epsilon}$, turning the cold plasma model into a "warm" one. As, from the numerical point of view, the "warm" model behaves very similar to the cold one we refrain here from using the former (except for Fig. 11).

Let us model a JET mode conversion scenario in a deuterium plasma with a central density $n_D(0) = 2.8 \cdot 10^{13}$ cm^{-3} and a small admixture of helium-3, $n_{He^3}(0) = 2.06 \cdot 10^{12}$ cm^{-3}. The density profiles are modelled by parabolas in the variable of $s = \sqrt{\psi}$ where ψ is the poloidal flux function. The toroidal magnetic field has a value of 3.4 T on the magnetic axis. The plasma current profile also is roughly parabolic with the safety factor on axis, $q_0 = 1$, and at the plasma boundary $q_a = 2.2$. The plasma beta is zero, since a force free equilibrium has been used. The phenomenological damping δ defined as in Ref. 12 is $\delta = 0.0025$.

The antenna is modelled as in our original AWRF work [18]: an imposed infinitely thin current sheet $\vec{J}_a = \vec{J}_a\delta(r-A(\theta))$ on an arbitrary toroidal surface, $r = A(\theta)$, encircling the plasma torus. Here r and θ stand for the minor radius and the poloidal angle, respectively. All wave quantities, and in particular the wave-exciting antenna current $\vec{J}_a$, are assumed to behave like $\exp(in\phi)$ in the toroidal direction. Apart from wave forms and absorption profiles in the plasma one wishes to compute the power emitted by the antenna [5],

$$P = \frac{1}{2}\int_{VACUUM} dV\, \vec{J}_a \cdot \vec{E}^* . \qquad (2)$$

A JET low-field-side (LFS) antenna is modelled by an antenna surface which approaches the plasma on the LFS and is near to the conducting wall elsewhere [5]. In this paper we do not sum over different components n of the antenna current, therefore not considering therefore, antennae with a finite toroidal extent. Except for the convergence studies we use throughout the paper $N_\psi = 160$ radial mesh points and $N_{pol} = 80$ poloidal mesh points.

In figure 1 we show contour lines of the circular left-hand polarisation of the electric field for the case of an exciting frequency, $f_0 = \omega/2\pi = 33$ MHz and a toroidal wave number, $n = -15$. Consequently, the "geometric" data for this case are the following : The cyclotron frequencies lie at $x = -64$ cm for D and at $x = 14$ cm for He^3 respectively, where x stands for the horizontal distance from the magnetic axis. The major and minor radii are 300 cm and 125 cm, respectively. The "homogeneous-plasma" mode conversion layer almost crosses the magnetic axis ($x = 3$ cm). As can be expected from general

considerations [19] the wave seems to be focussed to the center of the plasma and the local power absorption density, not shown here, has a large maximum in the center [5]. From this figure one could be tempted to believe that the energy leaving the antenna is focussed to the centre and is absorbed there in a single pass. However, this is not true at all. Looking at Fig. 1 more carefully we see that Alfvén resonances are excited near the high field side edge of the plasma. This means that the wave has been partly transmitted through the ion-ion hybrid mode conversion layer. Another indication comes from a plot of the total wave electric field and of the Poynting vector, not shown here, both of which show that the wave is not confined between the antenna and the mode conversion region, but is excited over the whole plasma cross-section.

A further indication comes from Fig. 2, where the total energy flux through a magnetic surface is shown versus the coordinate of that surface. We see that 50% of the energy is absorbed outside the surface $s_{1/2} = 0.36$. From the wavy structure for $s > 0.2$ of the power absorbed per radial interval we conclude that the wave is standing and that it suffers from the phenomenological damping. Apart from cases in which the electron Landau damping is large, this absorption is unphysical and can be avoided by tailoring the phenomenological damping.

The next fact is documented in Fig. 3 where we show a frequency scan of the power, Eq. (2), in the range of 31.2 to 34.8 MHz. Experimentally, such a scan is difficult to perform; however, evolving plasma parameters can change the physical situation in a similar way. Here we have chosen 33 MHz as a central frequency of the scan. We

intend to analyse the numerics for this very case in detail and, as it is in fact the physics which makes the case numerically delicate, we show its physical environs by changing the frequency. We have a certain sympathy for an unbiased reader's reaction on Fig. 3 who would qualify it as "computer hallucinations". It is, indeed, not obvious that the erratic behaviour of the power as a function of the frequency should be physical in nature. On earlier occasions [20], however, we had already found that frequency scans from a 2D-code can behave quite wildly when eigenmodes of the system are excited.

The JET experiment, in some cases, indeed shows variations of the loading impedance when the plasma parameters change and it is possible to interpret these variations as a scan of the spectrum of eigenfrequencies of the plasma column [3].

To make this point watertight we show in Fig. 4 the antenna loading, proportional to P, eq. (2), as obtained with the 1D-code ISMENE [14]. In a plane slab geometry we have used the same densities, magnetic field and geometric dimensions as for LION. No poloidal magnetic field is present. We have, on the other hand, used the hot plasma model with $E_z = 0$ and a central ion temperature of $T_i(0) = 2$ keV. The phenomenological damping [14] acting on the Bernstein wave was $\nu_B = 0.0005$. The poloidal wavenumber was $k_y = 0.02$ cm^{-1}. The equidistant mesh with 512 intervals together with the choice of cubic Hermite finite elements guaranteed well converged results [14]. As in Fig. 3 we find high resonance peaks in Fig. 4. There is no doubt that the antenna excites eigenmodes of the system at $f_o = 31.76$ MHz and at $f_o = 34.15$ MHz. The origin of the small peak is not completely

clear as yet. Its existence and height seem to be related to the relative position of the resonance and the nodes of the wave respectively [21]. The resemblance between the 1D and the 2D results is striking. It could even be more striking if in 1D we would sum over the different poloidal wavenumbers contained in the Fourier decomposition of the current in an antenna of the type shown in Fig. 1. This summation could result in a picture similar to Fig. 3 [3] where the peaks at 31.7, 33 and 34.2 MHz consist of several overlapping simple peaks.

The main features in Fig. 3 have thus found a physical explanation. Some features may or may not be of numerical origin. First of all, the toroidal resonances seem to be of lower quality that the ones in Fig. 4, which could be due to either the effect just mentioned or toroidal effects or a relatively high value of the phenomenological damping. Secondly, the peak at 33 MHz in Fig. 3 is more pronounced than the one in Fig. 4. Thirdly, the finescale hash on the loading curve can either be due to numerical problems or to the resonances with modes with different poloidal wavenumbers [3].

It is not easy to decide upon these questions because hitherto it has been impossible to perform hot-plasma computations of the quality of Fig. 4 in two dimensions. We must be satisfied with cold-plasma computations. When applied to large plasmas like JET and under weak absorption conditions (i.e. excitation of eigenmodes) even these computations are only marginally acceptable from a technical point of view of the numerics. It is one purpose of the next section to confront the reader with this fact.

Before we move on to these purely numerical questions in the next section, let us make a few final remarks on physics. In Fig. 5 is shown the wave field obtained with the new version of ISMENE for f_o = 33 MHz. Although this new version includes Landau damping we have been forced to use an additional phenomenological damping on the Bernstein waves of the order of ν_B = 0.00024 in order to prevent troubles in the region of the deuterium cyclotron resonance at X = -64 cm. The very short wavelength perturbation on the traces of E_x and E_z in this region is a numerically converged signal (a non-equidistant mesh has been used) but it is physically meaningless because the wavelength is of the order of the deuterium Larmor radius and, hence, the theory used is not valid. When we shall analyze the numerics and be tempted to feel unsatisfied we should keep in mind even the limitations of the physics. The situation is dissimilar from that in ideal MHD stability where the physical model seldom needs to be criticized and all the forces can be concentrated on the numerical techniques.

As a last point we note in Fig. 5 that the fast magnetosonic wave, best characterized by the trace of E_y, seems to ignore the mode conversion layer. Evidently, this cannot be true. A close inspection of the phases shows that the wave on the HFS of the conversion layer is strictly standing as it should be: there is no energy transport there. An additional inspection of the traces of Im E, not shown here, reveals moreover that $E_+ = E_x + iE_y \approx 0$ on the HFS as already remarked in Fig. 1.

2.3 Numerical techniques for the cold plasma model

In the cold plasma model there is no essential formal difference between the singularities leading to resonance absorption of the fast magnetosonic wave at the Alfvén and ion-ion perpendicular resonances [12,22]. It seems therefore to be obvious that one would use the same numerical techniques in the ICRF as in the AWRF.

In MHD stability [23] and in AWRF studies [24] our slogan has always been "spectral pollution". When the ideal MHD operator is discretized with standard finite element methods, one obtains a very bad numerical representation of the continuous spectra associated with the mentioned singularities. Spurious discrete eigenfrequencies appear outside the frequency band occupied by the continua. The discrete spectrum is "polluted" by modes which have been ejected from the continuum by the improper discretization and, as a consequence, the continuous spectrum has lost modes and has become "more discrete". Pollution can spoil any ideal MHD stability calculation. The implications for RF-computations in the AWRF have been assessed in Ref. 24 and will here be discussed for the ICRF. In Ref. 24 we have found that, if more mesh points are used, a polluting method can produce results of similar quality as a non-polluting one .

The importance of the discretization technique for RF heating applications can be emphasized by two additional points. It can be shown [25] that in the plane slab geometry the wave fields must behave like

$$E_x \sim 1/|x-x_s|, \quad E_y \sim \log|x-x_s| \qquad (3)$$

in the neighbourhood of the singularity at x_s. The numerical discretization should allow for this behaviour or at least

$$dE_y/dx \sim E_x, \tag{4}$$

i.e. if a piecewise linear continuous approximation is used for E_y, the component E_x is better approximated by piecewise constant than by piecewise linear functions.

Moreover, the analytical treatment of the problem yields a Poynting flux which is constant from the antenna up to the conversion layer (the singularity) and is zero beyond. In the limit of vanishing phenomenological damping, the transition is discontinuous and the numerical approximation should allow for this discontinuity which indeed it does when E_x is piecewise constant. The discontinuity in E_x can also be illustrated by Fig. 5: in the mode conversion region E_x changes its phase relative to the continuous E_y.

For more detailed information let us experiment with five different discretization procedures in one dimension. We define an arbitrary non-equidistant, spatial mesh by

$$x_o < x_1 < \ldots < x_j < \ldots < x_n, \tag{5}$$

where x_o and x_n are the left and the right plasma boundary [14].

We shall need the four following finite element basis functions: the piecewise constant basis functions,

$$\gamma_{j+\frac{1}{2}}(x) = \begin{cases} 0, & x \leq x_j, \\ 1, & x_j < x < x_{j+1} \\ 0, & x_{j+1} \leq x, \end{cases} \tag{6}$$

the piecewise linear basis functions

$$\sigma_j(x) = \begin{cases} 0, & x \leq x_{j-1}, \\ \dfrac{x - x_{j-1}}{x_j - x_{j-1}}, & x_{j-1} \leq x \leq x_j, \\ \dfrac{x_{j+1} - x}{x_{j+1} - x_j}, & x_j \leq x \leq x_{j+1}, \\ 0, & x_{j+1} \leq x, \end{cases} \tag{7}$$

and the two piecewise cubic basis functions

$$\psi_j(x) = \begin{cases} 0, & x \leq x_{j-1}, \\ \sigma_j^2(x)\left[3 - 2\sigma_j(x)\right], & x_{j-1} \leq x \leq x_{j+1}, \\ 0, & x_{j+1} \leq x, \end{cases} \tag{8}$$

and

$$\varphi_j(x) = \begin{cases} 0, & x \le x_{j-1}, \\ \sigma_j^2(x)\,[x - x_j], & x_{j-1} \le x \le x_{j+1}, \\ 0, & x_{j+1} \le x. \end{cases} \qquad (9)$$

Here, we merely have space to note the different finite element expansions. For details see refs. 14 and 23.

Method 1 is the standard expansion in cubic Hermite elements [14]:

$$\vec{E}(x) = \sum_{j=0}^{N} (e_x^j, e_y^j)\,\psi_j(x) + \sum_{j=0}^{N} (f_x^j, f_y^j)\,\varphi_j(x). \qquad (10)$$

Here $(e_x^j,\ e_y^j)$ and $(f_x^j,\ f_y^j)$ are the nodal values of $\vec{E}$ and $d\vec{E}/dx$ respectively.

Method 2 is the standard expansion in linear finite elements [14]:

$$\vec{E}(x) = \sum_{j=0}^{N} (e_x^j, e_y^j)\,\sigma_j(x). \qquad (11)$$

These two methods lead to spectral pollution because E_x and E_y are

approximated by functions with the same regularity. A conforming [23] non-polluting approximation is obtained in Method 3:

$$E_x = \sum_{j=1}^{N} e_x^{j-\frac{1}{2}} \gamma_{j-\frac{1}{2}}(x) ,$$

$$E_y = \sum_{j=0}^{N} e_y^{j} \sigma_j(x) . \qquad (12)$$

Method 4 and Method 5 are based on the same non-conforming approximation ("finite hybrid elements" [23])

$$E_x = \sum_{j=1}^{N} e_x^{j-\frac{1}{2}} \gamma_{j-\frac{1}{2}}(x) ,$$

$$E_y = E_y^{(1)} = \sum_{j=1}^{N} e_y^{j-\frac{1}{2}} \gamma_{j-\frac{1}{2}}(x) ,$$

$$\frac{dE_y}{dx} = \frac{dE_y^{(2)}}{dx}$$

where

$$E_y^{(2)} = \sum_{j=0}^{N} c_y^{j} \sigma_j(x) . \qquad (13)$$

Note that in the case of a cold plasma with $E_z = 0$ the variational form of eq. (1) does not contain derivatives of E_x. The expansion coefficients $e_y^{j-\frac{1}{2}}$ and c_y^{j} of E_y are constrained by

$$\int (E_y^{(1)} - E_y^{(2)}) \gamma_{i+\frac{1}{2}}(x)\,dx = 0, \quad \forall\ i = 1, \ldots, N, \tag{14}$$

which leads to $e_y^{j+\frac{1}{2}} = (c_y^j + c_y^{j+1})/2$.

The discretized variational form of eq. (1) leads to a linear system for the expansion coefficients. The matrix elements are of the form

$$A_{ij} = \int \rho_i(x)\, F(x)\, \tilde{\tau}_j(x)\,dx \tag{15}$$

where $\rho_i(x)$ and $\tau_j(x)$ are basis functions and $F(x)$ is a coefficient of the differential equation (1).

The value of A_{ij} is obtained numerically with a nine-point formula for the Methods 1 to 4. The nine-point formula is compulsory for Method 1 if the degree of accuracy of the cubic elements is to be preserved by the quadrature. Simpson's rule would be sufficient for Methods 2 and 3 and the trapezoidal rule for Method 4. This is just the difference between Method 4 and Method 5: in Method 5 the trapezoidal rule has been used for the evaluation of A_{ij}. Methods 4 and 5 are trivially different as long as the coefficients $F(x)$ are continuous. In the ICRF problem, however, they are discontinuous across the points where $\omega = \omega_{ci}$, where ω_{ci} is a cyclotron frequency. For large values of N Methods 4 and 5 have nevertheless yielded the same results. Method 5 is the 1D analogue of the approximation used in the

2D code LION. It is equivalent to a centered finite difference scheme.

Before we compare Methods 1, 2, 3 and 5 let us first investigate the influence of a phenomenological damping Δ which, for simplicity and in contrast to the 2D case, is added directly to S as given in Stix's book [11]:

$$\varepsilon_{xx} = \varepsilon_{yy} = S + i\Delta. \tag{16}$$

The relation between Δ and the one used in the 2D calculations, δ, is

$$\Delta = 2\delta c^2/c_A, \tag{17}$$

where c_A stands for the local Alfvén velocity: with δ = const, Δ is roughly proportional to the density.

In Fig. 6 we show the same frequency scan as in Figs. 3 and 4 but obtained with Method 1 on a very fine equidistant mesh (N = 6000) for three different values of Δ, viz. Δ = 1, 3 and 10. The resemblance between the trace obtained with the hot plasma model in Fig. 4 and the one here obtained with Δ = 1 is very striking. Apart from the region between 32.8 and 33.1 MHz the circles in Fig. 6 fall on the trace in Fig. 4. We conclude that the cold plasma model can reproduce the results obtained with the hot model.

Comparing Figs. 3 and 6 we find that the shape of the 2D trace is very similar to the 1D trace obtained with Δ = 10. The artificial damping, δ = 0.0025, used in 2D corresponds roughly to $\Delta \approx 5[1-(x/a)^2]$

where a is the minor radius. The average Δ is smaller than 5. One could therefore be tempted to expect the 2D trace to be similar to the $\Delta = 3$ rather than to the $\Delta = 10$ trace in 1D. From this point one would further conclude that the different poloidal modenumbers contained in the 2D model lead to a broad compound peak. This conclusion is premature: in 2D the artificial damping could be more effective in broadening the resonance peaks because the volume occupied by the mode conversion region is, compared to the total plasma volume, smaller than in 1D. Most probably both effects are operative.

There is an additional feature in Fig. 6 which needs to be discussed. We mean the badly scattered $\Delta = 1$ data points in the region of 32.9 MHz which are the heralds of numerical problems. Imagine: we have used 6000 mesh points for this calculation and still the result seems not to be well converged. How can one hope to produce reasonable results with the 2D code where at most we have $2N_\psi = 400$ points across the plasma? How wrong can the results be?

A partial answer can be obtained from Fig. 7 where again frequency scans of the loading impedance are presented. These computations have been performed with methods 1, 2, 3 and 5 on a $N = 512$ equidistant mesh with $\Delta = 1$. The vertical scale is logarithmic. The continuous line shown as a reference in all four graphs is the trace obtained with the hot plasma model (Fig. 4). The three peaks of Fig. 4 are reproduced here by all four methods. All the methods produce, however, a few additional peaks which are numerical in nature. The most embarrassing one is the peak at 32.35 MHz on the trace (b) obtained with regular linear finite elements. This peak is neatly described by

data points and really looks physical. Even the ones at 33.3 MHz on the traces (c) and (d) do not look too unphysical.

We seem to be in the presence of two problems here: one of them is pollution and can be avoided, and the other is insufficient resolution and is, in the 2D context, unavoidable. Without an additional extensive investigation of traces like in Fig. 7 it is difficult to know what exactly is ascribable to one or the other or both. In a very pragmatic way we could comment Fig. 7 in the following way.

As Methods 3 and 5 (traces c and d) yield practically the same results we need to compare merely methods 1, 2 and 5. Method 2 (trace b) is a polluting method and the results are correspondingly bad. The non-polluting Method 5 shows less numerical peaks than the polluting Method 1, the difference in quality being, however, not extraordinary. We could even say that, in fact, all the methods yield equally bad results. It is then easy to choose the "best method". Method 5 is the most rapid and the least memory-occupying procedure. It permits the use of much finer meshes than the Methods 1 and 2. As an example, a computation with N = 6000 and Method 1 uses 988K words and 21.4 secs CPU time on CRAY 1 as compared with 436K words and 2.2 secs with Method 5.

Let us further comment the results shown in Fig. 7. Most of the non-physical peaks are probably just due to insufficient resolution and are easy to understand from the spectral point of view. All the exciting frequencies in Fig. 7 lie in the continuum of eigenfrequencies associated with the ion-ion perpendicular resonance. Accept-

able numerical results can only be expected if the eigenfrequencies of the discretized system are sufficiently dense, meaning that their spacing $\Delta\omega$ in the region of the exciting frequency ω is smaller than the damping produced by Δ. In the opposite case, modes in the continuum behave like discrete modes and lead to resonance peaks on the antenna loading. There are, hence, two ways of avoiding spurious peaks: one either increases Δ or decreases $\Delta\omega$ by increasing the mesh density around the ion-ion perpendicular resonance.

These two points are documented in Fig. 8 where a convergence study is shown for the case f_o = 33 MHz on an equidistant (a+b) and on two different non-equidistant meshes (c+d). The different methods of discretization have been used. Traces a, c and d have been obtained with Δ = 1, the value used in Fig. 7. In contrast, Δ = 3 has been used for trace b. On the equidistant meshes with a reasonable size (N > 256) the non-polluting methods show somewhat less variation than the polluting ones consistent with our expectation. There is, however, not the sligthest sign of a convergence law. At N > 256 the variation with Δ = 3 (trace b), however, is clearly much smaller than with Δ = 1 (trace a). Clear convergence can be obtained with non-equidistant meshes. For trace c we used a spatial mesh size of Δx = 0.3 cm/N around the ion-ion perpendicular resonance whereas in d) it was Δx = 0.5 cm/N. From traces c and d it is clear that the choice of a non-equidistant mesh requires a certain experience: in trace c too many mesh points have been wasted for the resonance and are not available for the description of the overall wave function. A judicious choice of the non-equidistant mesh permits good convergence for N > 128. On the non-equidistant meshes the cubic elements (Method 1)

perform extremely well. The conclusion that for a 2D application Method 5 is the best, however, still holds for two reasons. First of all, in 2D the mesh cannot be adapted to the same degree as in 1D. Secondly, the Poynting flux obtained with the cubic elements can show very strong overshoot in the region of the resonance and hence would be difficult to interpret in a complex 2D situation.

What more have we learned that could be useful in judging the performance of the 2D code LION and, afterall, of any 2D code [1,2] based on the cold plasma model for ICRF ? The situation investigated in Fig. 3 is dominated by eigenmodes. This is a situation difficult to model numerically because the height of some peaks is strongly affected by the phenomenological damping Δ, Fig. 6. The damping Δ with which it is possible to simulate the hot plasma, Fig. 4, is too small from the numerical point of view : in a large-size plasma like JET and with a number of equally spaced mesh points typical for a 2D model it is impossible to describe well all the continuous spectra, Fig. 7. In a 1D model one can have resort to nonequidistant meshes. In the 2D case, however, this is possible only to a limited degree because, in general, there are several resonances to be correctly described (see e.g. Fig. 13 in Ref. 5).

We must therefore be pleased to see in Fig. 9 that the convergence behaviour of the 2D model is much better than one could expect from the 1D analysis. Note that here we have used linear vertical scales again. The 2D problem seems to be a bit less delicate to treat than the 1D problem. The reason is probably the same as for which we cannot use highly nonequidistant meshes : there is a multitude of

different coupled resonances and they have a certain averaging influence.

In conclusion, we can say that the "hybrid finite elements" are the best choice for a 2D code and that such a code can reasonably be used for the assessment of an ICRF heating scenario which is dominated by eigenmodes in a large machine. On a computer like CRAY 1, however, such a code cannot be used yet as a black box because the spatial resolution is only marginally sufficient. A corollary is that the credibility of a hot plasma model [15] in 2D is even more in question.

3. Quasilinear Evolution of Distribution Functions

3.1 Physical background

The most commonly used numerical approach to RF current drive is what has become known as Fokker Planck Codes [26,27] in one and two dimensions. These codes solve an equation for species α of the form

$$\frac{\partial f_\alpha}{\partial t} + \frac{\partial}{\partial \vec{v}} \cdot \vec{S}_w + \frac{q_\alpha}{m_\alpha} \vec{E} \cdot \frac{\partial f_\alpha}{\partial \vec{v}} = \sum_{\alpha'} C(f_\alpha, f_{\alpha'}), \qquad (18)$$

where $f_\alpha(\vec{v},t)$ is the particle distribution function, q_α and m_α the charge and mass of species α, $\vec{E}$ the D.C. electric field associated with the loop voltage in tokamaks and $C(f_\alpha,f_{\alpha'})$ is a collision operator describing collisions between particles of the species α and α'. The wave induced flux, $\vec{S}_w$, is obtained from quasilinear theory by

$$\vec{S}_w = - \vec{\vec{D}} \cdot \frac{\partial f_\alpha}{\partial \vec{v}} \qquad (19)$$

where $\vec{\vec{D}}$ is the quasilinear diffusion tensor, the form of which depends on the type of waves present in the plasma.

Most of the investigations into current drive published so far assume the quasilinear diffusion tensor to be given. One good reason for this assumption is that then the problem, eq. (18), is amenable to numerical and semianalytical calculations. Often the full non-linear collision operators, which conserve momentum and energy, are used in these models. This is, however, an inappropriate complication because energy transport in configuration space is not included in eq. (18). Energy put into the system by either the DC electric field (Ohmic heating) or by the RF waves has no way to go [26] and therefore the models with energy conserving collision operators have to be supplemented by an ad hoc energy loss term in order to make them capable of describing steady states. It is, therefore, equally good to use simple linear collision operators with a "heat bath". These operators drive f_α back to a Maxwellian of a given temperature.

Equation (18) is essentially a diffusion-advection equation. As long as the driving electric field is small as compared with the total diffusion coefficient (due to the collision and the RF) the equation is easy to solve. The only delicate situation is that of electron runaway, where in a certain velocity range the advective term dominates over the diffusive terms. If the resolution is not sufficient it is common that the front of a runaway tail exhibits strong numerical

ripples. These ripples might prevent one from an accurate evalutation of the runaway rate.

The situation drastically changes when one tries to include more physics into eq. (18) by allowing for the self-consistent evolution of $\vec{\vec{D}}$, eq. (19). The diffusion tensor $\vec{\vec{D}}$ is then schematically given by

$$\vec{\vec{D}} = \sum_{\nu} \int d^3k \, W(\vec{k}, t) \, \vec{\vec{\Lambda}}(\vec{k}) \, \delta\left(\omega(\vec{k}) - k_{\parallel} v_{\parallel} - \nu \Omega_c\right), \quad (20)$$

where ν is a sum over cyclotron harmonics, $\vec{k}$ are the wave vectors of the injected and eventual internally created unstable waves with the spectral distribution $W(\vec{k},t) \sim |\vec{E}_{\vec{k}}(t)|^2$, $\vec{\vec{\Lambda}}(\vec{k})$ is a time invariant tensor depending on the type of waves present and $\omega(\vec{k})$ is the frequency of these waves. The wave vector and the velocity have components $k_{\parallel}$ and $v_{\parallel}$ parallel to the equilibrium magnetic field. The wave intensity evolves according to an equation of the form

$$\frac{\partial W}{\partial t} = \left(2\gamma_{ql} - \nu_{coll}\right) W + Q(\vec{k}) \quad (21)$$

where the quasilinear growth rate, γ_{ql} is a functional of f_{α}, ν_{coll} is the collisional damping of the wave and $Q(\vec{k})$ is an external RF source that has been extensively used for current drive studies [28,29].

The reader might ask why at all we intend to deal with the difficulties of the full quasilinear equations (18)-(21) when the simple Fokker-Planck equation, (18), together with an imposed wave induced flux, $\vec{S}_w$, is sufficient to model current drive. The sad fact is that

we still do not know [30] for sure why LHRF current drive works so sucessfully [31,32,33]. As in the past [34] the Fokker-Planck codes correctly predict efficiencies, i.e. the ratio of the produced current to the invested power, but they fail in predicting the right magnitude of current and power individually. The discrepancy between the calculated currents and the observed ones is even larger today [33]. Moreover, most of the dynamical behaviour, where observed, is poorly understood. For these reasons we should remain open-minded and investigate physics in a broad sense; the quasilinear theory is a part of it.

A quasilinear code allows one to study the self-consistent, dynamical behaviour of both the wave spectral and the particle velocity distribution functions. The dynamical behaviour includes situations like LHRF current ramp-up, DC electric field and/or LHRF wave induced runaways and associated instabilities, beam instabilities and related subjects. As a by-product, in a quasilinear code one only needs to specify the spectral shape of an energy source, $Q(\vec{k})$, and not that of an energy density, $W(\vec{k})$, as in a Fokker-Planck code. This point is important in situations where ray-tracing codes predict a multitude of reflections [35] of the injected rays.

3.2 Some remarks on the numerical techniques

The quasilinear code ADLER presented at this conference [6] is in fact a 4D code, the 4 dimensions being $v_{\parallel}$, $v_{\perp}$, $k_{\parallel}$ and $k_{\perp}$, the components of $\vec{v}$ and $\vec{k}$ parallel and perpendicular to the equilibrium magnetic field. Nevertheless the problem is amenable to numerical calcu-

lation at least as long as one limits the wave-particle interaction to resonant interactions of the type shown in eq. (20).

Equations (18)-(21) are discretized on rectangular grids :

$$
\begin{aligned}
&-\infty < v_{\parallel}(0) < v_{\parallel}(1) < \cdots < v_{\parallel}(i_{\parallel}) < \cdots < v_{\parallel}(N_{\parallel}) < \infty ,\\
&0 = v_{\perp}(0) < v_{\perp}(1) < \cdots < v_{\perp}(i_{\perp}) < \cdots < v_{\perp}(N_{\perp}) < \infty ,\\
&k_{\parallel}(1) < k_{\parallel}(2) < \cdots < k_{\parallel}(j_{\parallel}) < \cdots < k_{\parallel}(M_{\parallel}) ,\\
&k_{\perp}(1) < k_{\perp}(2) < \cdots < k_{\perp}(j_{\perp}) < \cdots < k_{\perp}(M_{\perp}) .
\end{aligned}
\tag{22}
$$

The unknown functions f and W are expanded in finite elements defined on these grids :

$$f(v_{\parallel}, v_{\perp}, t) = \sum_i f_i(t)\, \tau_i(v_{\parallel}, v_{\perp}), \tag{23}$$

$$W(k_{\parallel}, k_{\perp}, t) = \sum_j W_j(t)\, \rho_j(k_{\parallel}, k_{\perp}), \tag{24}$$

where i and j stand for a numbering of the pairs $(i_{\parallel}, i_{\perp})$ and $(j_{\parallel}, j_{\perp})$. For the 2D basis functions in velocity space we have taken,

$$\tau_i(v_{\parallel}, v_{\perp}) = \sigma_{i_{\parallel}}(v_{\parallel})\, \sigma_{i_{\perp}}(v_{\perp}), \tag{25}$$

and for those in the k-space either

$$\rho_j(k_{\parallel}, k_{\perp}) = \sigma_{j_{\parallel}}(k_{\parallel})\, \sigma_{j_{\perp}}(k_{\perp}) \tag{26}$$

or

$$\varrho_j(k_\parallel, k_\perp) = \gamma_{j_\parallel + \frac{1}{2}}(k_\parallel)\, \gamma_{j_\perp + \frac{1}{2}}(k_\perp). \qquad (27)$$

We shall again show that the piecewise constant approach, eq. (27), has a definite advantage over that using linear finite elements, eq. (26).

Before doing so let us explain the numerical difficulty engendered by the resonant wave-particle interaction. This interaction couples the two "populations", f and W, weakly in the sense that a cell in k-space, C, interacts only with a narrow strip in v-space defined by eq. (20) or by

$$v_\parallel = \frac{\omega(\vec{k}) - \nu\Omega_c}{k_\parallel} \qquad \text{for} \quad k_\parallel \in C. \qquad (28)$$

It is this very fact that allows us to treat an essentially 4D problem. On the other hand, it causes numerical troubles because abrupt changes in k-space lead to abruptly changing coefficients in v-space, eq. (18). These alone and eventually in conjunction with the advective action of a DC electric field tend to produce numerical ripples on the distribution function. These, in turn, can trigger instabilities via the quasilinear growth, $\gamma_{ql} \sim \partial f_\alpha / \partial v_\parallel$, and can falsify the physics or even bring the time evolution to a stop when the abrupt changes in k-space are amplified.

These considerations led us to believe that a smooth higher order finite element expansion would help us to avoid the mentioned

problems. As a first step in this direction, in ADLER we started off with a smoother approximation, eqs. (24) and (26), for W than that previously used, eq. (27), or in the terminology of Chapter 2, we tried the 2D analogue of Method 2 instead of Method 4. The result was disappointing. This is documented with a simple calculation in Fig. 10.

In Figure 10 we show the evolution of the wave spectral distribution on a coarse mesh with a fixed particle distribution. At time $t = 0$ (the time is normalized to ω_{pe}, the plasma frequency) we had $W = 1$ in arbitrary units. In eq. (21) the only term included was $\gamma_{q\ell}$ which was positive in the region $0.14 \leq k \leq 0.184$. With the automatic time step control in action we have performed 200 time steps with Method 2 and 30 time steps with Method 4. The final results are shown in Fig. 10b. An intermediate situation is shown in Fig. 10a. We see that Method 2 leads to strong overshoot which, in the worst case when $W < 0$, could even lead to negative diffusion in eq. (18). On finer meshes Method 2 clearly behaves more reasonably but we have always been able to advance in time much faster with Method 4. The problem seems to be connected with the boundary between stability and instability: whereas in the piecewise constant approximation the growth rate of a grid point is simply given by the integral of the growth rate over the mesh cell C, it is connected via the mass matrix to all the other grid points when the piecewise linear approximation is used. This connection is unnecessary and even detrimental in the discretization of a trivial equation like eq. (21). Near the stability boundary the small nodal values of stable points tend to change erratically from step to step by a large relative amount due to this global connection and a reduction of the time step results.

We can conclude that here again the piecewise constant approach performs better than the regular linear finite elements. It remains to be seen whether it is advantageous to abandon the linear elements (Method 2) even for the discretization of the particle distribution function, eqs. (23) and (25).

4. Application

4.1 TCV (Tokamak à Configuration Variable)

Our laboratory plans the construction of a new tokamak with large elongation and the question has been posed of how such a machine would best be heated by low-frequency RF waves. It is clear that ICRF from the LFS would be as viable a method as on any other machine. The particular question addressed here is whether it would be possible to install the antennae below and above (T/B: top-bottom) rather than on the LFS. Especially in the AWRF we are anxious about the energy being absorbed near to the plasma surface when this antenna position is used.

We have made a superficial first investigation of this question. The parameters used are $n_D = 2.10^{14}$ cm^3, 7.35% He-3, $B_o = 1.43$T, $q_o = 1.05$, $q_a = 2.12$, $\beta = 2.8\%$, major radius 87.5 cm, minor radius 24 cm and an elongation of 2.5. In Fig. 11 we compare the position $s_{1/2}$ of the minor radius inside which half of the total power is absorbed for the two antenna positions in the two frequency ranges.

Concerning the AWRF we find it difficult to deposit the energy into the plasma interior but there are a few quite acceptable T/B cases. The case f_o = 1.3 MHz with n = -4 T/B antenna is shown in Fig. 12. As far as the antenna position is concerned, to our astonishment the highly-elongated plasma behaves very similar to the plasma with a circular cross-section [18]: one can reach better the plasma interior with a T/B configuration than with an LFS configuration and moreover the ratio of reactive to resistive antenna load (not shown here) on the average is smaller in the T/B case. Here one seems, however, to be forced to use higher toroidal mode numbers, e.g. n = -4, whereas in the circular case acceptable results can be obtained with n = -2.

Concerning the ICRF mode conversion heating the LFS antenna position seems to be clearly favourable but the T/B position yields still better penetration than any of the AWRF scenarii. The same conclusion can be drawn from both plasma models used.

The scatter of the data points in the ICRF T/B case with cold plasma probably is of numerical nature. On the other hand, the scatter seen in the AWRF results is of physical origin and has to do with the subsequent appearance of new resonant surfaces in the plasma.

4.2 Production of runaways in LHRF ramp-up

Recent current-drive experiments in PLT and ASDEX [36,37] have clearly demonstrated the ability of lower-hybrid waves not only to

maintain a steady plasma current, but also to increase it ("ramp-up") during the discharge. Since the time variation of the current induces a DC electric field opposite to the direction of RF waves, any appropriate theoretical description of current ramp-up requires the knowledge of the plasma dynamical response to the simultaneous application of the RF power and opposing electric field.

In a short conference contribution [38] we have recently investigated the dynamical behaviour of the plasma current. As a by-product we have found steady states with runaway tails higher than predicted by the "classical" theory [39].

Here, we investigate this effect in detail. In Fig. 13 we have plotted the runaway rate $A = (d\rho/dt)\,(\rho\nu_{ei})^{-1}$ as a function of the electric field measured in units of the Dreicer field, $E_D = m_e v_{the}\nu_{ei}/e$, where v_{the} is the electron thermal speed $(T_e/m_e)^{1/2}$, ν_{ei} the electron-ion collision frequency and

$$\rho = 2\pi \int_{-v_B}^{v_B} dv_\parallel \int_0^{v_B} v_\perp \, dv_\perp \, f_e \quad . \tag{29}$$

In our computations $v_B = 15\ v_{the}$. We have used a discretization with $(N_\parallel, N, M_\parallel, M) = (80, 30, 10, 20)$ and the k-space was limited by $0.01 \leq k_\parallel\lambda_D \leq 0.2$ and $0.04 \leq k\lambda_D \leq 0.4$ where λ_D denotes the Debye length. The LHRF waves have a Gaussian spectrum [29] and act in velocity space in the range $3.5\ v_{the} \lesssim v_\parallel \lesssim 10\ v_{the}$. The total power corresponds roughly to the PLT ramp-up conditions [36]

of about 130 kW. The electric field acts in the opposite direction and accelerates runaway electrons towards $v_{\parallel} = -\infty$.

In Fig. 13 we show the runaway rate with and without RF as obtained with ADLER. As a reference line we have also drawn the result obtained from analytical theory without RF [39]. If the fields are such, $0.02 \lesssim E/E_D \lesssim 0.16$, that the critical velocity $v_c/v_{the} \approx (2E_D/E)^{1/2}$, lies approximately within the range of phase velocities of the LHRF waves, the latter are even capable of enhancing the runaway rate in the opposite direction because a certain amount of LH produced high energy electrons are collisionally pitch-angle scattered from $v_{\parallel} > 0$ to $v_{\parallel} < 0$ [40] and run away if their velocity is higher than v_c. Their presence on the way from positive to negative $v_{\parallel}$ can best be demonstrated by the shape of the distribution function at $v_{\parallel} = 0$: $f_e(v_{\parallel} = 0, v_{\perp})$, Fig. 14.

In the past we have treated LHRF and runaway problems with a quasilinear model in which the shape of the distribution function was assumed to be Maxwellian in v . With such a model it is impossible to treat LHRF anti-runaway situations as the one just presented. The effect demonstrated in Figs. 13 and 14 is a real 2D effect and can only be treated consistently with a model like ADLER.

5. Conclusion

We have discussed certain aspects of the numerical modeling of RF heating and current drive. The physical problems treated are such that

the numerical resolution is marginal. In such a situation - and this is a trivial conclusion - it is worth trying different methods of discretization with the aim to find the "best". For the physical problems investigated we have found that the "finite hybrid elements" were by far the best concerning efficiency: for equal memory space and central processor times the results obtained with the hybrid elements were "nearer" to the correct results than those obtained with regular linear or cubic finite elements. In realistic cases we were, however, unable to demonstrate convergence laws. In such a situation - and this is a non-trivial conclusion - it is worth disposing of different methods of discretization in one and the same computer code. In the absence of convergence laws, the use of these different methods permits an assessment of the discretization errors, and provides credibility to the numerical approach.

Acknowledgement

We thank R. Bartiromo, D. Düchs, R. Gruber, J. Jacquinot, P. Lallia, F. Leuterer, F. Marcus, F. Parlange and F. Troyon for discussions. This investigation was partly supported by the Swiss National Science Foundation. The part concerning ICRF has been carried out under the JET Article 14 contract No. JT4/9007.

References

[1] Proc. 3rd Europ. Workshop on Problems in the Numerical Modeling of Plasmas (NUMOP 85), Varenna, Sept. 1985. Invited papers in Computer Physics Reports, August 1986.

[2] Proc. of NUMOP 85. Contributed papers in Comput. Phys. Commun. 40 (1986) 1-157.

[3] T. Hellsten and K. Appert, Proc. 13th Europ. Conf. on Contr. Fusion and Plasma Heating, Schliersee, April 1986, paper Mo-24.

[4] R. Bartiromo, LH- and ASDEX-Teams, ibid., paper Th-01.

[5] L. Villard, K. Appert, R. Gruber and J. Vaclavik, to appear in Ref. 1.

[6] S. Succi, K. Appert and J. Vaclavik, paper contributed to this Conference.

[7] P. Brossier, Nucl. Fus. 18 (1978) 1069.

[8] G. Melin et al., Proc. Int. Conf. Plasma Phys., Lausanne, 1984, Invited Papers, Vol. I, p. 225.

[9] M. Brambilla, to appear in Ref. 1.

[10] K. Appert, J. Vaclavik and L. Villard, Phys. Fluids 27 (1984) 432.

[11] T.H. Stix, The Theory of Plasma Waves (McGraw-Hill, New York, 1965).

[12] K. Appert et al., Plasma Phys. and Contr. Fusion 28 (1986) 133.

[13] H.L. Berk and R.R. Dominguez, J. Plasma Phys. 18 (1977) 34.

[14] K. Appert, T. Hellsten, J. Vaclavik and L. Villard, in Ref. 2.

[15] A. Fukuyama, K. Itoh and S.-I. Itoh, in Ref. 1.

[16] T. Martin and J. Vaclavik, "Dielectric Tensor Operator of a Nonuniformly Magnetized Inhomogeneous Plasma", Lausanne Report, LRP259/85, 1985.

References (cont'd)

[17] R. Gruber et al., Comput. Phys. Commun., 21 (1981) 323.

[18] K. Appert et al., Nucl. Fusion 22 (1982) 903.

[19] C.K. Phillips, F.W. Perkins, D.Q. Hwang and D.G. Swanson, in Ref. 2.

[20] K. Appert, R. Gruber, F. Troyon and J. Vaclavik, Plasma Phys. 24 (1982) 1147.

[21] K. Appert, J. Vaclavik and L. Villard, Proc. 11th Europ. Conf. Contr. Fusion and Plasma Phys., Aachen 1983, Contributed Papers, Part I, p. 305.

[22] T. Hellsten and E. Tennfors, Physica Scripta 30 (1984) 341.

[23] R. Gruber and J. Rappaz, "Finite Element Methods in Linear Ideal Magnetohydrodynamics", (Springer, Berlin, 1985).

[24] K. Appert et al., Comput. Phys. Commun. 24 (1981) 329.

[25] K. Appert, J. Vaclavik and L. Villard, "Lecture Notes: An Introduction to the Theory of Alfvén Wave Heating (with a side-glance on ICRF)", Lausanne Report, LRP238/84, 1984.

[26] C.F.F. Karney, in Ref. 1.

[27] In Ref. 2: pp. 123, 137 and 153.

[28] S. Succi, K. Appert, J. Vaclavik and D. Moreau, in "Plasma Physics and Controlled Nuclear Fusion Research, 1984" (IAEA, Vienna, 1985) Vol. 1, p. 549.

[29] S. Succi, K. Appert and J. Vaclavik, Plasma Phys. and Contr. Fusion 27 (1985) 863.

[30] S. von Goeler et al., Nucl. Fusion 25 (1985) 1515.

[31] J. Hosea, Proc. 13th Europ. Conf. on Contr. Fusion and Plasma Heating, Schliersse, April 1986. Invited paper to appear in Plasma Phys. and Contr. Fusion.

References (cont'd)

[32] C. Gormezano, ibid. invited paper.

[33] F. Leuterer, LH- and ASDEX-Teams, ibid., contributed paper Th-24.

[34] J. Vaclavik et al., Plasma Phys. 25 (1983) 1283.

[35] P. Bonoli and E. Ott, Phys. Fluids 25 (1982) 359.

[36] F.C. Jobes et al., Phys. Rev. Lett. 55 (1985) 1295.

[37] F. Leuterer et al., Phys. Rev. Lett. 55 (1985) 75.

[38] S. Succi, K. Appert and J. Vaclavik, Proc. 13th Europ. Conf. on Contr. Fusion and Plasma Heating, Schliersee, April 1986, paper TH-23.

[39] V.V. Parail and O.P. Pogutse, Nucl. Fusion 18 (1978) 303.

[40] N.J. Fisch, private communication.

Figure Captions:

Fig. 1: Contour lines of the circular left-hand polarization of the electric field, $|E_+|$, for a mode conversion scenario in JET in a deuterium plasma with 7.35% of He-3 and a frequency of f_o = 33 MHz.

Fig. 2: Energy flux (- - - -) through a magnetic surface, labelled with $s = \phi^{1/2}$, and power absorbed per radial interval Δs (————) versus s for the case shown in Fig. 1.

Fig. 3: Power (in normalized units) emitted by the antenna versus frequency for the scenario of Fig. 1 as obtained with the 2D model LION.

Fig. 4: Antenna load Z versus frequency as obtained with the hot plasma model in 1D (ISMENE).

Fig. 5: The real parts of the wave fields versus the spatial coordinate as obtained with the new version of ISMENE. Same parameters as for Fig. 1.

Fig. 6: Antenna load Z versus frequency as obtained with the cold plasma model in 1D on a fine mesh with N = 6000. Cubic elements. Three different phenomenological dampings have been used: Δ = 1 (0), Δ = 3 (———) and Δ = 10 (- - - -).

Fig. 7: Antenna load Z versus frequency as obtained with the cold plasma model in 1D on a coarse equidistant mesh with N = 512 and Δ = 1. Four different discretization methods have been used:

a) cubic elements, b) linear elements, c) conforming, non-polluting elemets and d) non-conforming, non-polluting elements. The continuous reference line is identical to that in Fig. 4.

Fig. 8: Convergence behaviour of the antenna load versus mesh size for the four different methods shown in Fig. 7: cubic elements (————), linear elements (‾‾‾‾), conforming, non-polluting elements (••••) and non-conforming, non-polluting elements (‾‾‾‾). The meshes are equidistant in cases a) and b) and non-equidistant in c) and d). The phenomenological damping is Δ = 1 except for case b) where Δ = 3.

Fig. 9: Convergence behaviour of the power emitted by the antenna and the magnetic surface $s_{1/2}$ inside which 50% of the emitted energy is absorbed versus the mesh size in the 2D case.

Fig. 10: Wave spectral distribution, W, versus the absolute value of the wave vector, k, as obtained with linear elements (————) in 200 steps and with finite hybrid elements (‾‾‾‾) in 30 steps, case b), whereas case a) is an intermediate situation.

Fig. 11: Position of the magnetic surface, $s = s_{1/2}$, within which 50% of the energy is absorbed for the two frequency ranges AWRF and ICRF (mode conversion) in the planned tokamak TCV. Antenna position is either top/bottom (T/B) or low field side (LFS). In the AWRF different toroidal mode numbers have been used: $n = -2$ O and $n = -4$ ● . In the ICRF different absorption models have been used: Cold plasma ■ and "warm plasma" □ (ion-cyclotron absorption of fast magnetosonic wave included).

Fig. 12: Contour lines of the power absorption density in TCV for the AWRF case with the best power absorption profile, i.e. $n = -4$, $f_0 = 1.3$ MHz. 42% of the energy are deposited on the innermost layer and 38% on the next one. The remaining 20% are absorbed at $s > 0.8$.

Fig. 13: The runaway rate, A, versus the electric field E measured in units of the Dreicer field, E_D. Shown are the prediction of the analytical theory (- - - -) and the numerical results (————). High values of "anti-runaway" are obtained when high energy electrons are produced by LHRF current drive. Case $E/E_D = 0.04$ (0) is analyzed in Fig. 14.

Fig. 14: Electron distribution function, $f_e(v_\parallel = 0, v_\perp)$, along the $v_\perp$ -axis as a function of the perpendicular energy. The LHRF current drive results in a long tail even in $v_\perp$. The critical velocity corresponding to $E/E_D = 0.04$ is situated in the tail, leading to enhanced runaway.

Fig. 1

Fig. 2

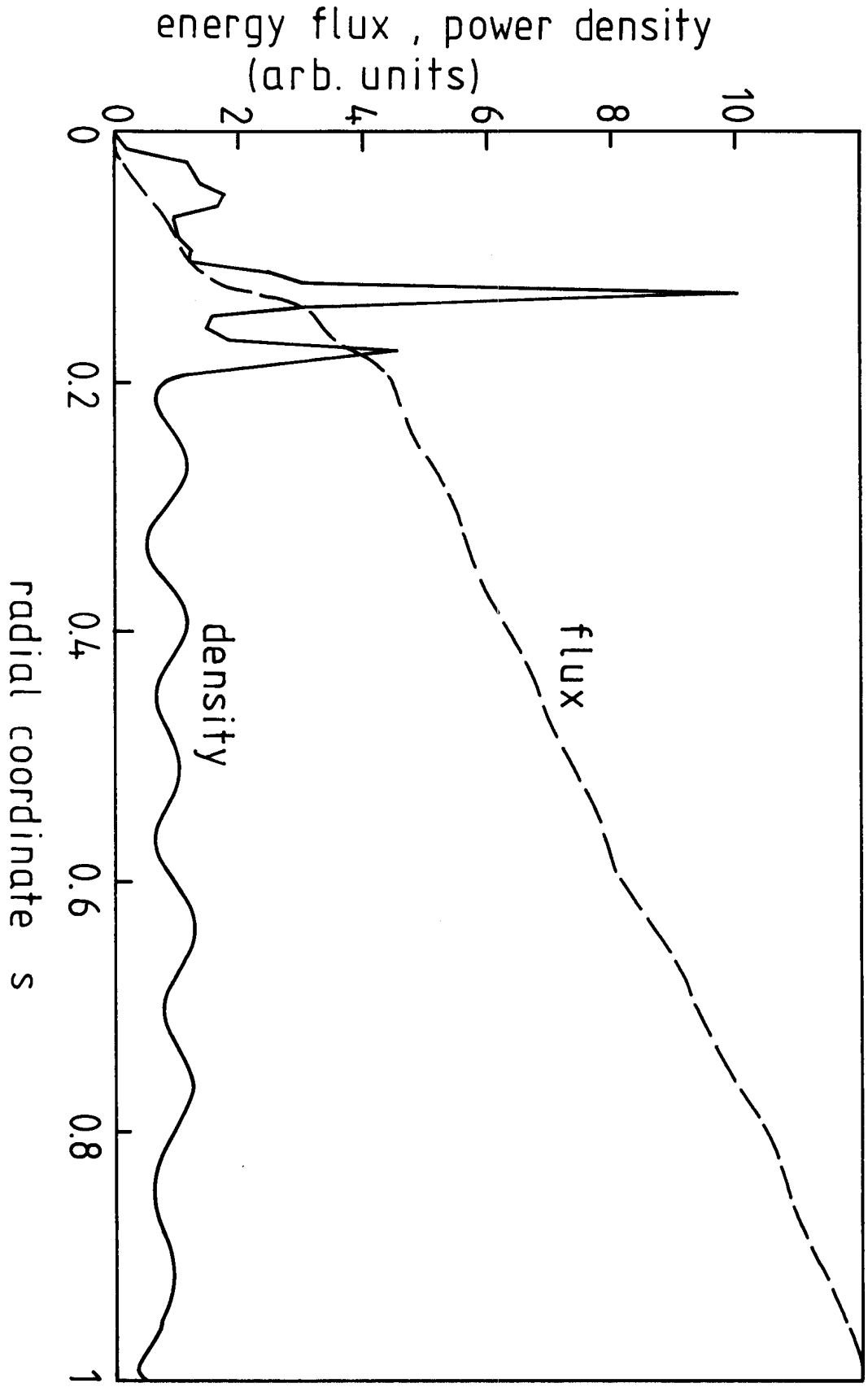
energy flux , power density
(arb. units)
0
2
4
6
8
10
0
0.2
0.4
0.6
0.8
1
radial coordinate s
density
flux

Fig. 3

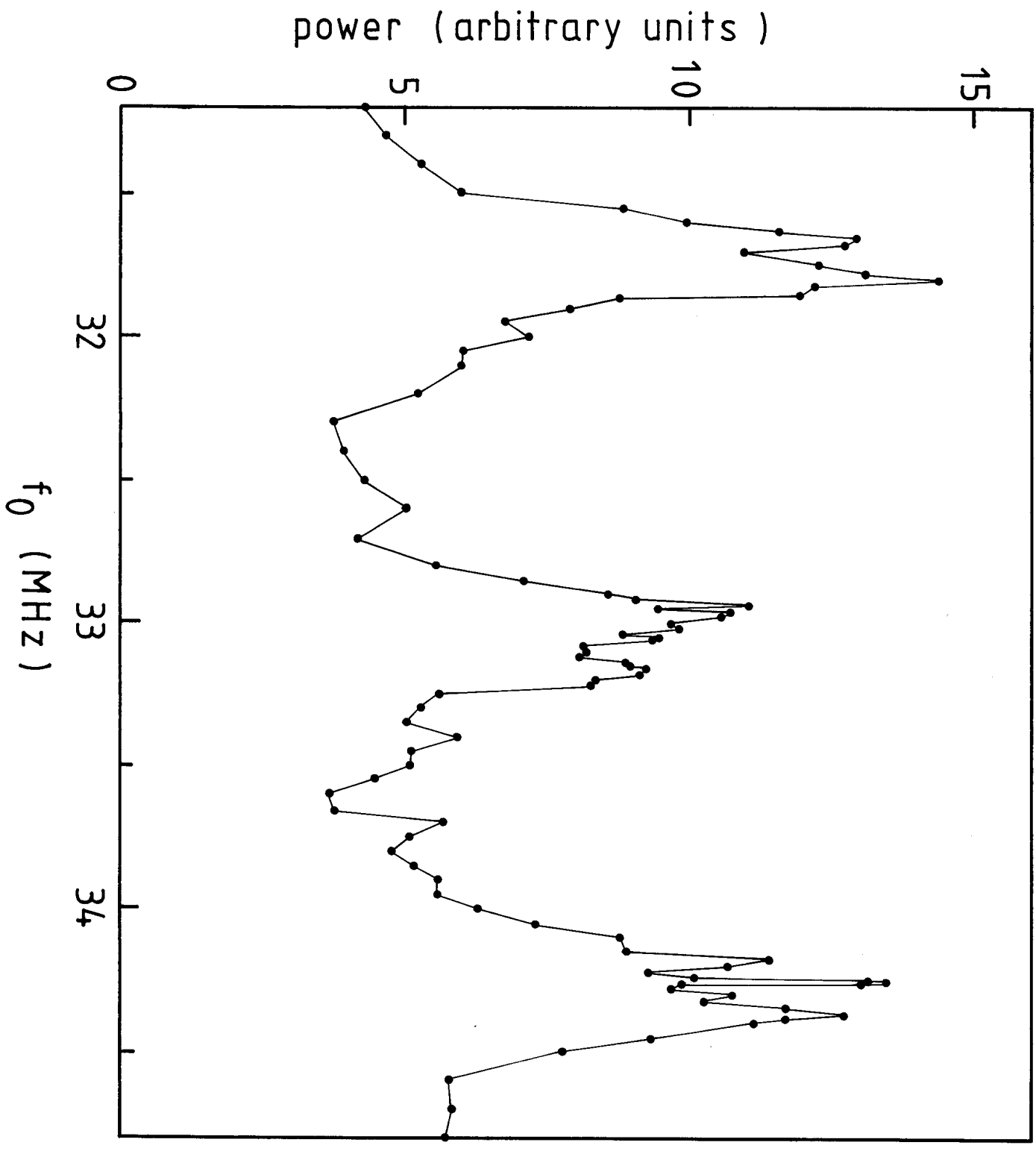

Fig. 4

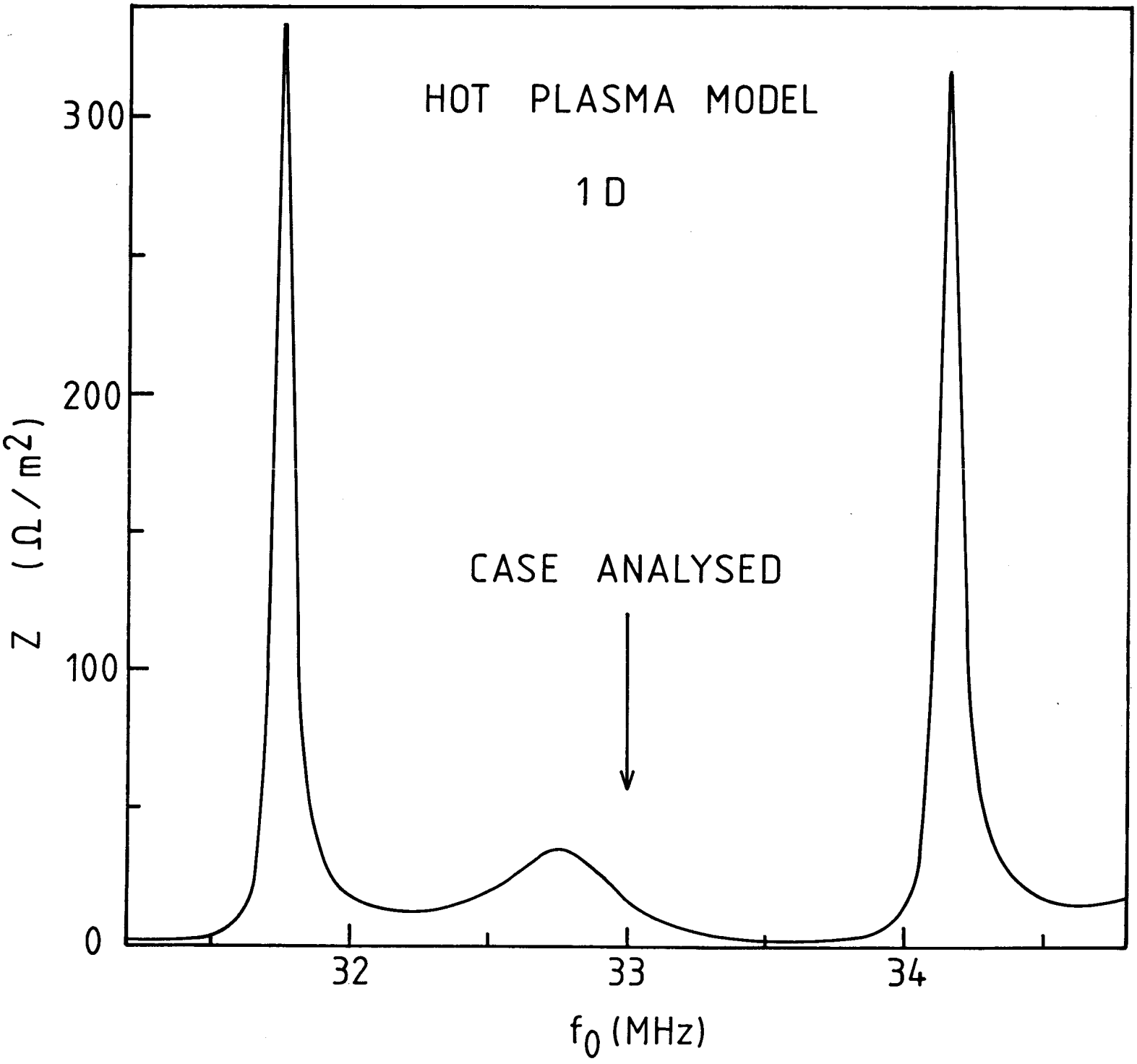
HOT PLASMA MODEL
1 D
CASE ANALYSED
300
200
100
0
Z (Ω / m²)
32
33
34
f0 (MHz)

Fig. 5

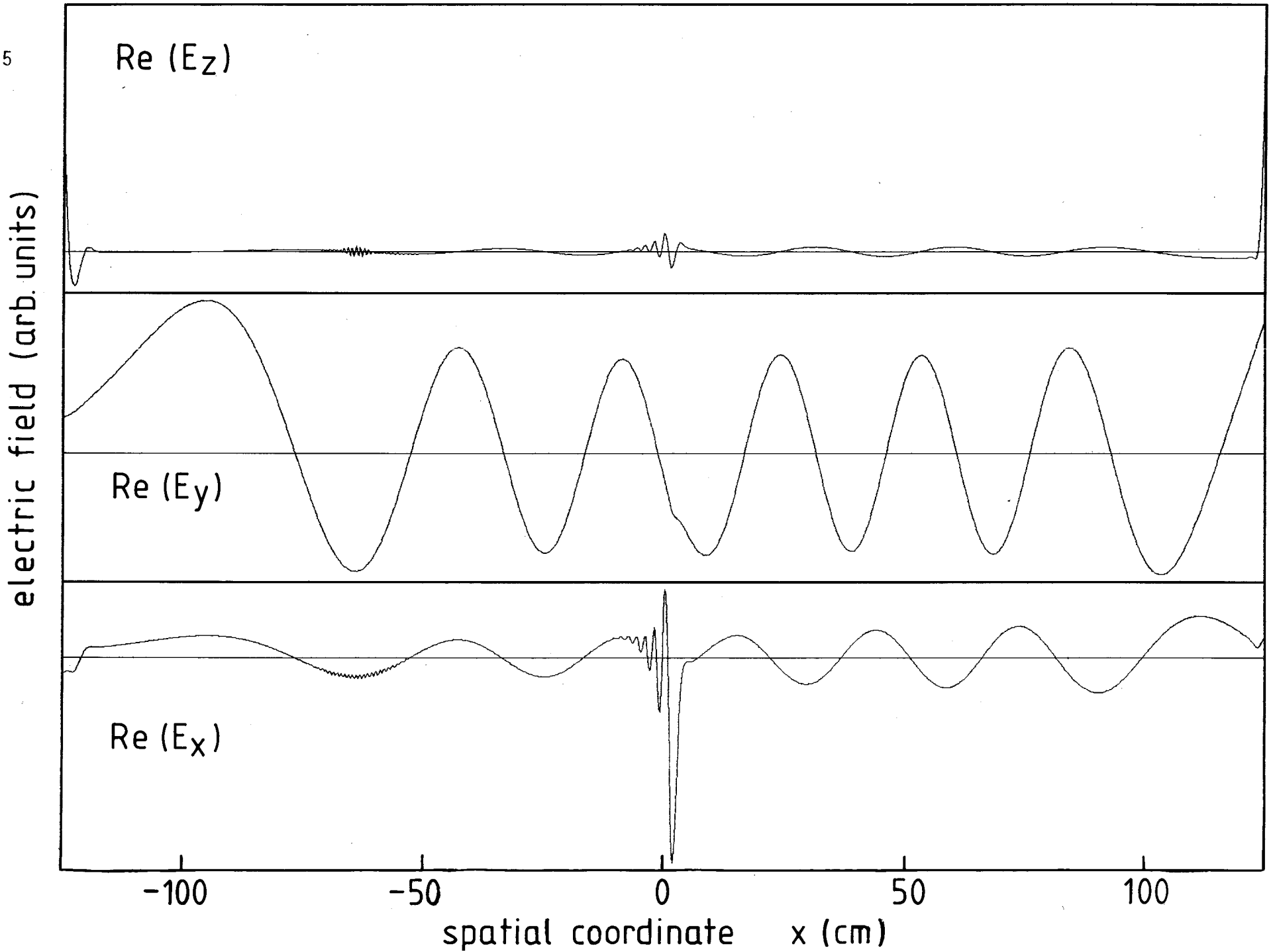
Re (Ez)
Re (Ey)
Re (Ex)
electric field (arb. units)
-100
-50
0
50
100
spatial coordinate x (cm)

Fig. 6

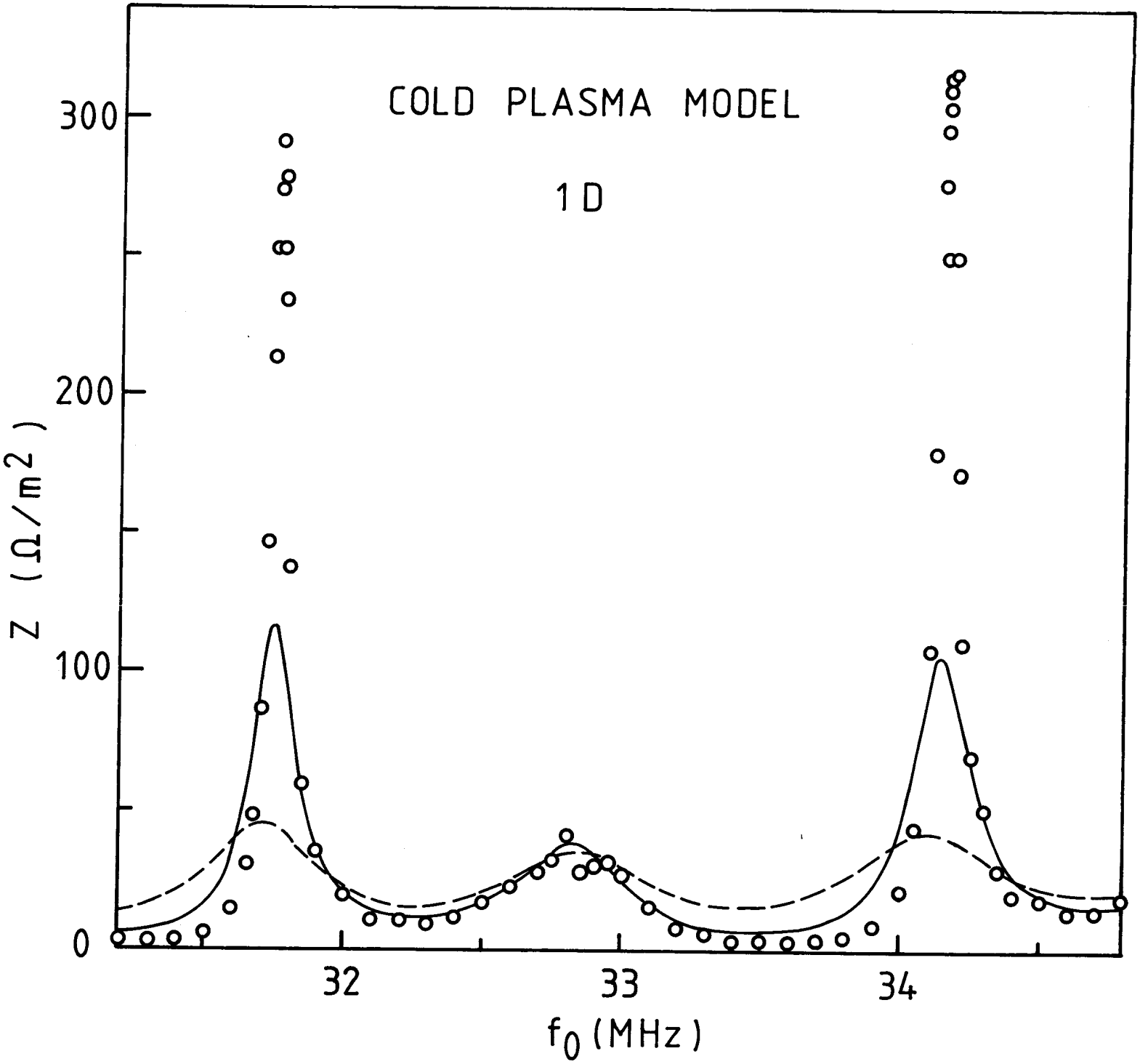

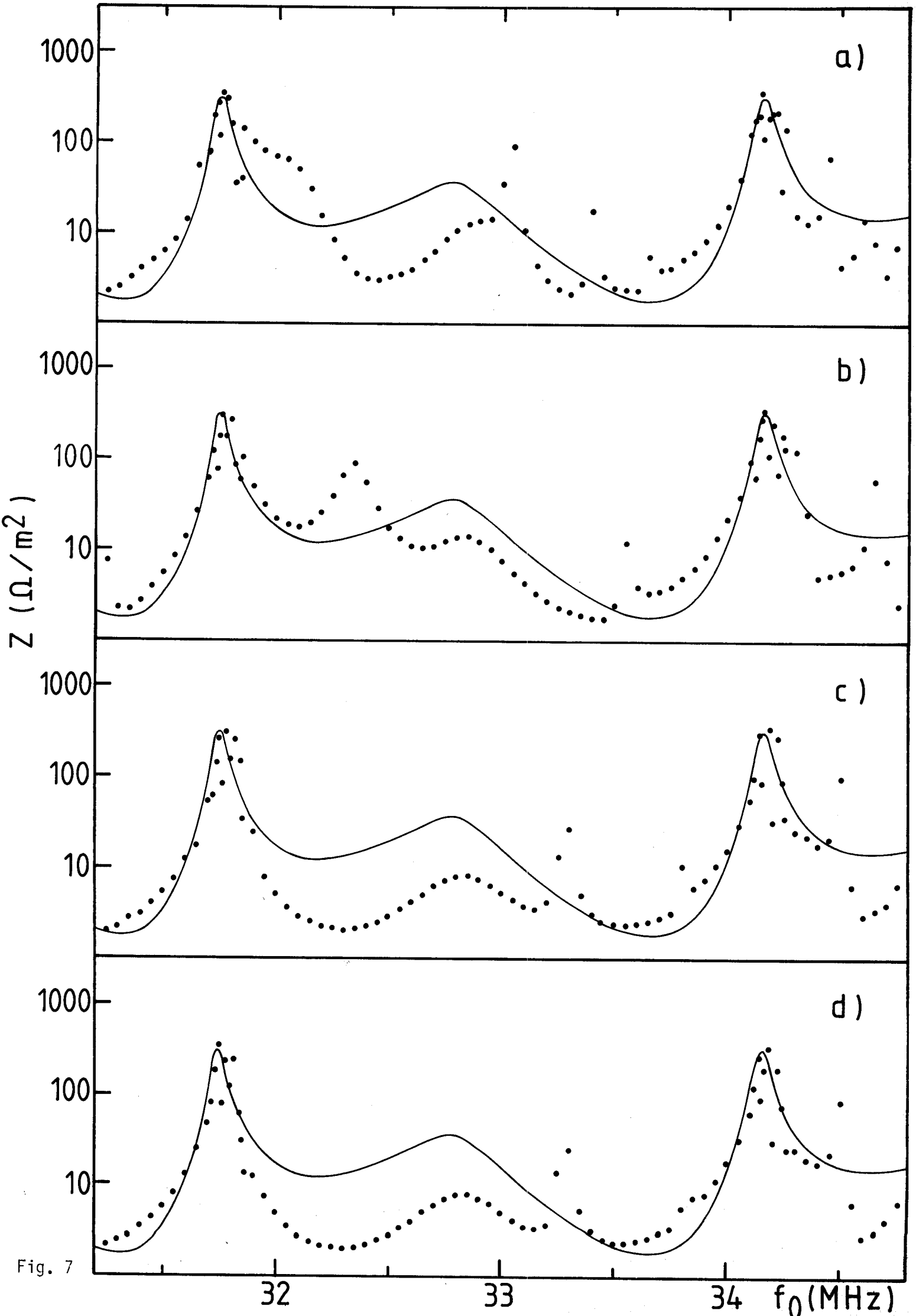

Fig. 7

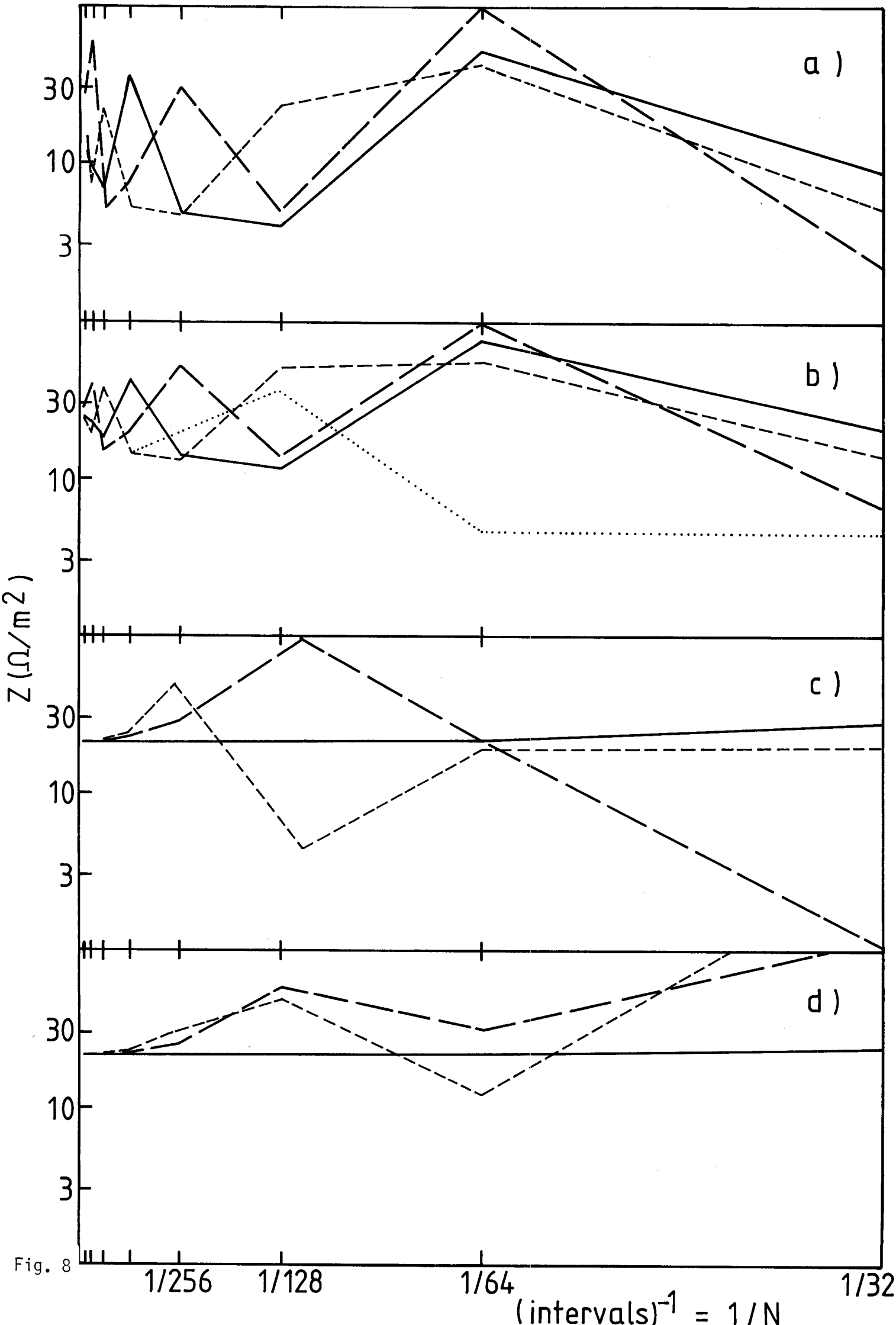

Fig. 8

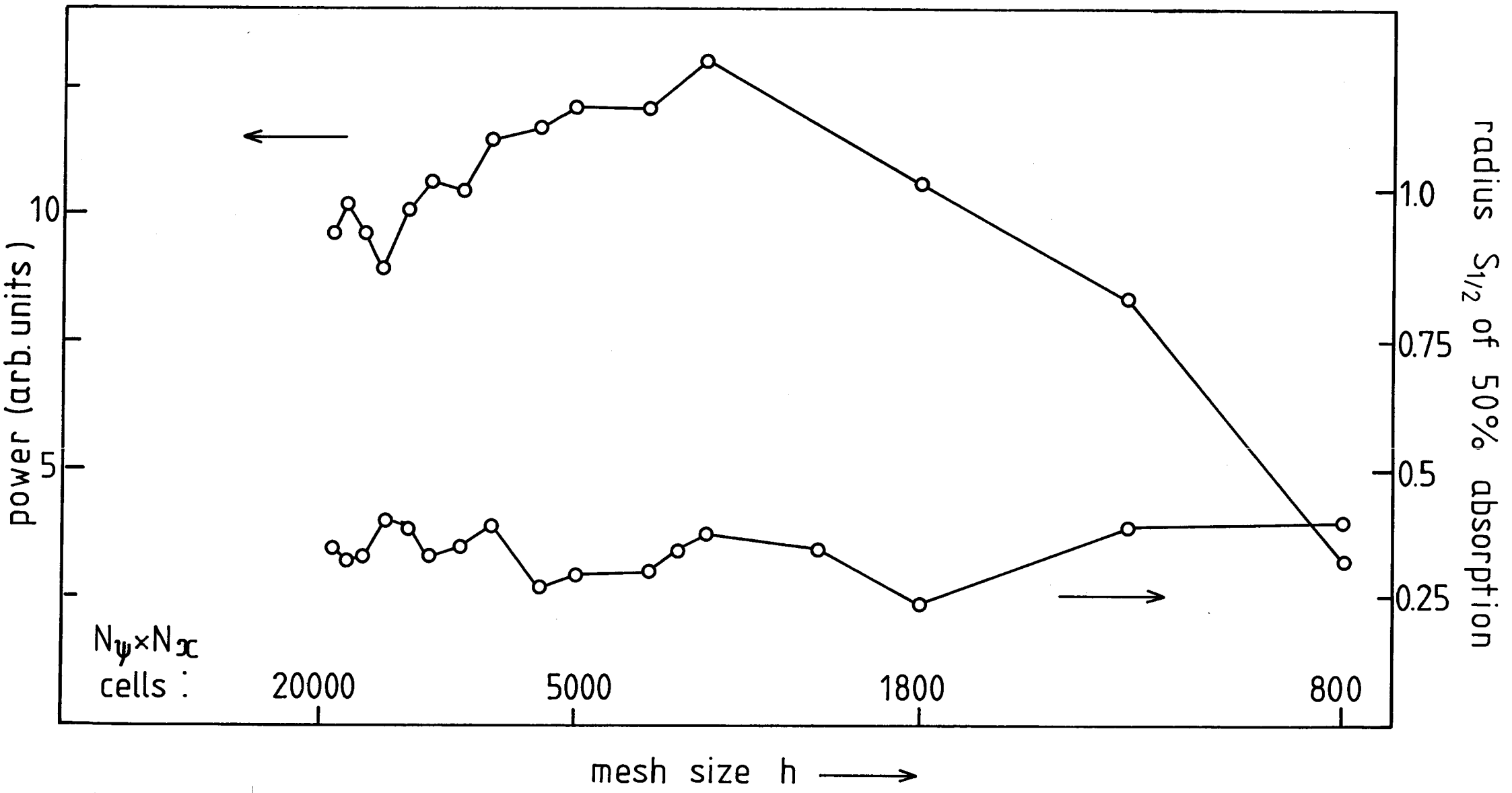
power (arb. units)
10
5
radius $S_{1/2}$ of 50% absorption
1.0
0.75
0.5
0.25
$N_\psi \times N_\chi$
cells :
20000
5000
1800
800
mesh size h

Fig. 9

Fig. 10

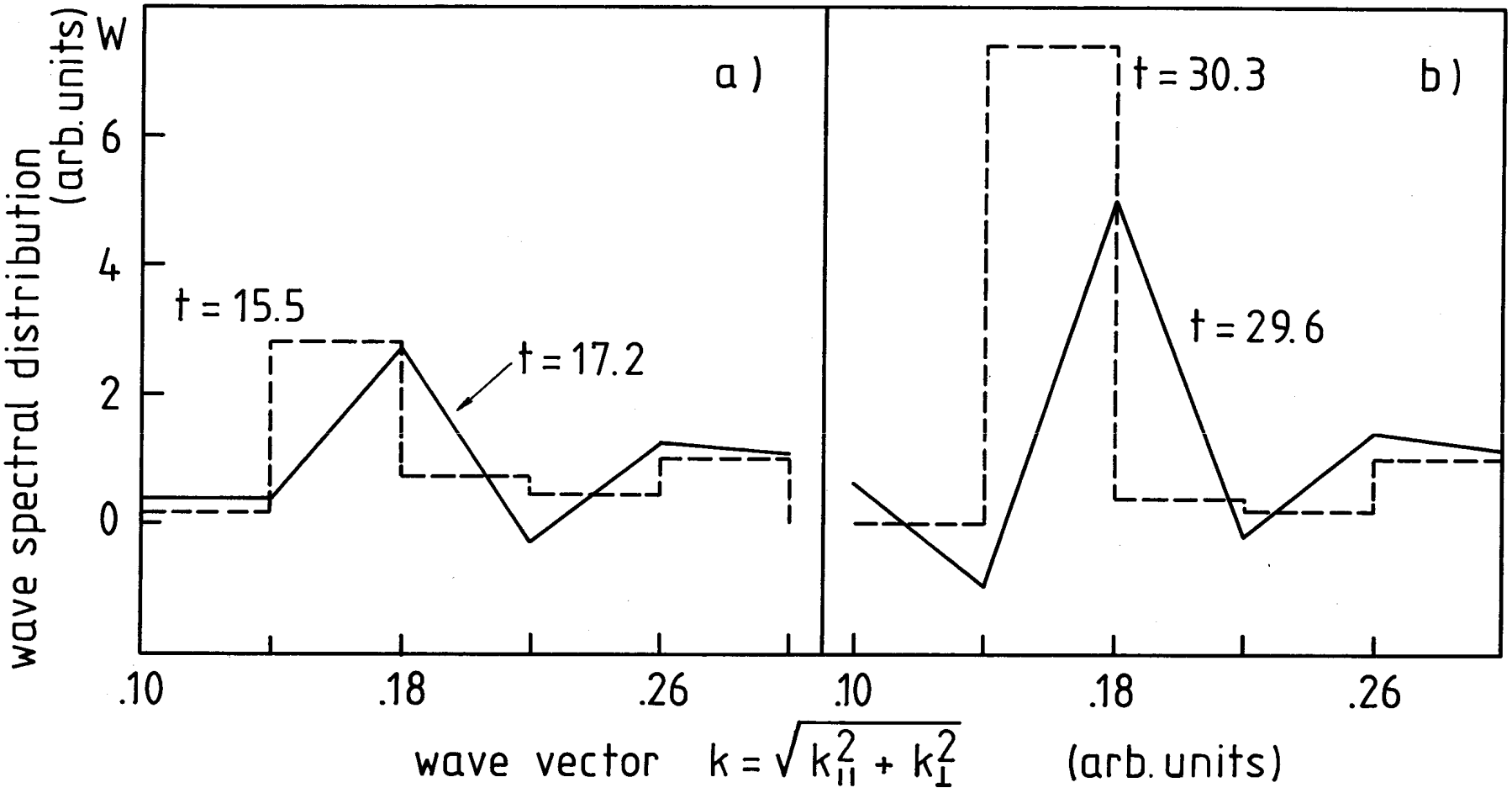
wave spectral distribution (arb. units)
W
6
4
2
0
a)
b)
t = 15.5
t = 17.2
t = 30.3
t = 29.6
.10
.18
.26
.10
.18
.26
wave vector $k = \sqrt{k_{\parallel}^2 + k_{\perp}^2}$
(arb. units)

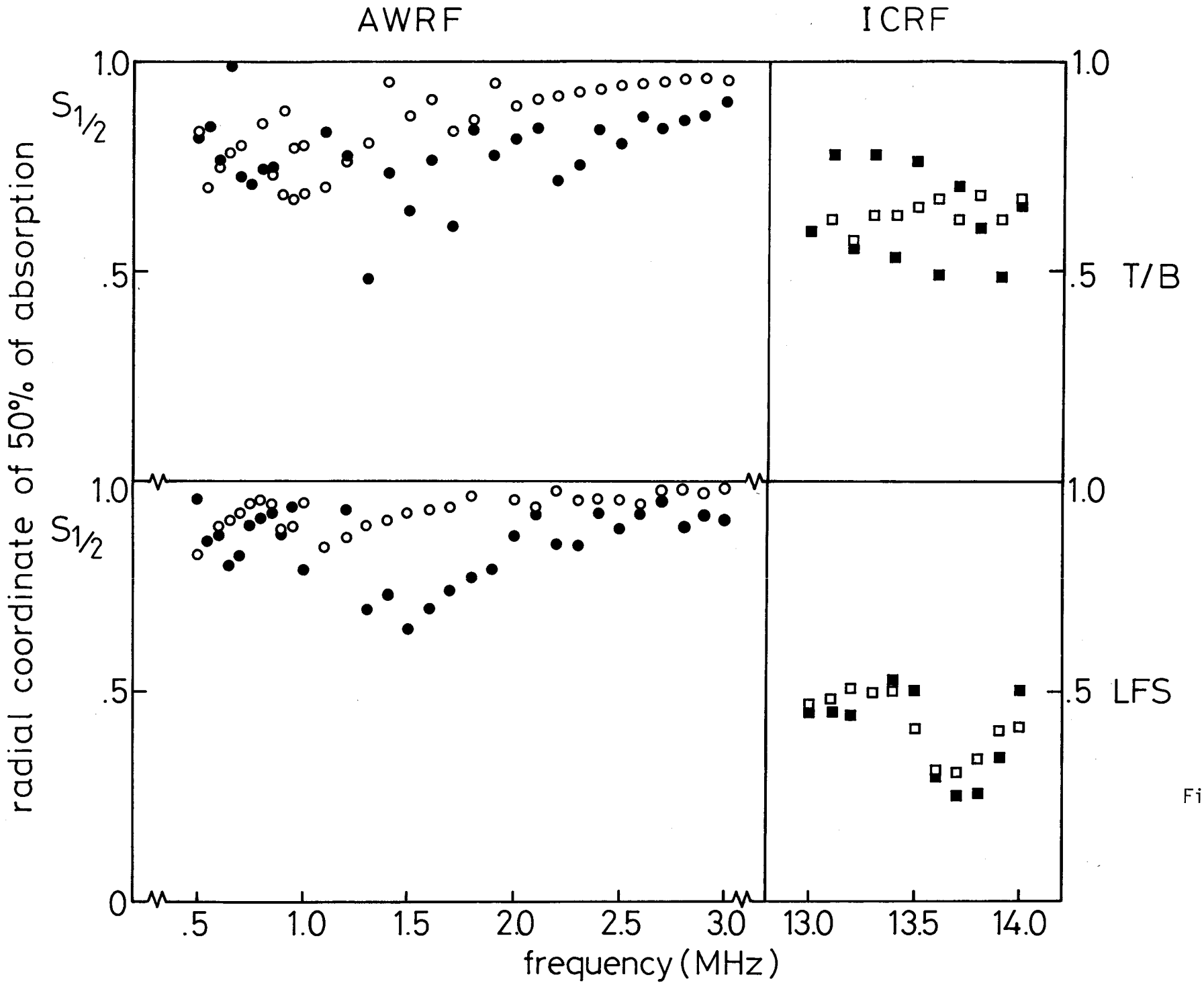
AWRF
ICRF
1.0
$S_{1/2}$
.5
1.0
$S_{1/2}$
.5
0
1.0
.5 T/B
1.0
.5 LFS
radial coordinate of 50% of absorption
.5
1.0
1.5
2.0
2.5
3.0
13.0
13.5
14.0
frequency (MHz)

Fig.11

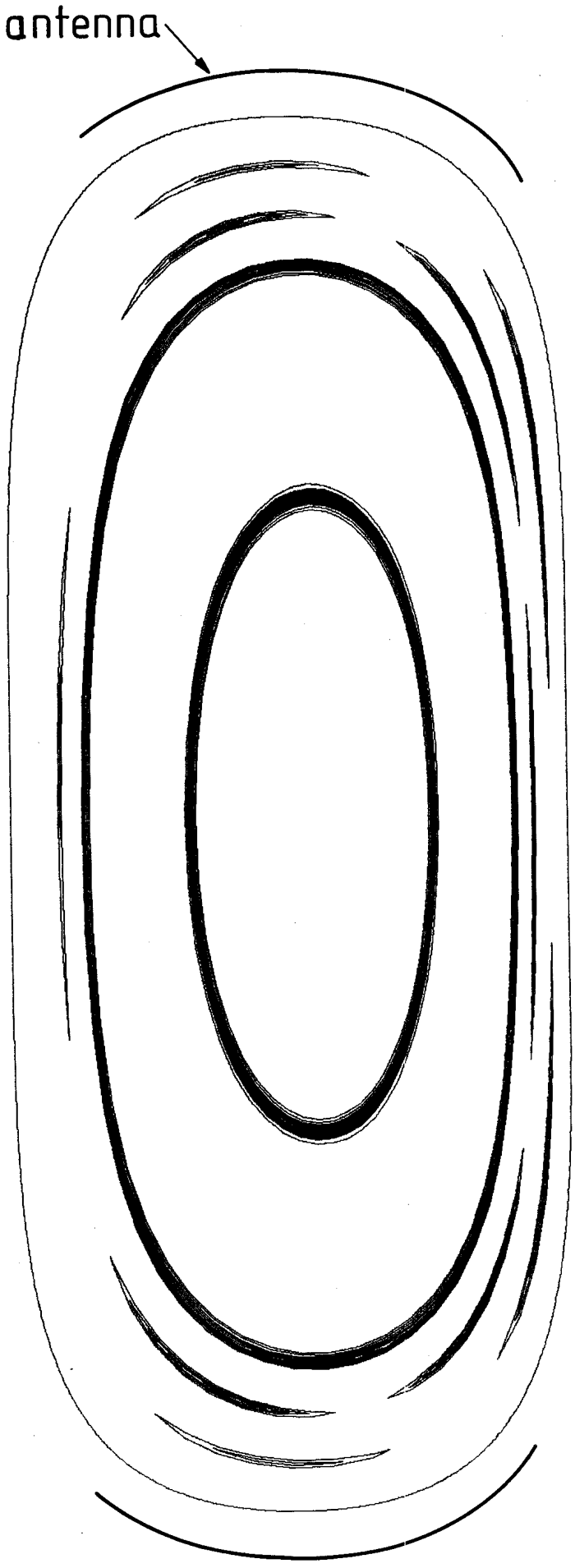

Fig. 12

Fig. 13

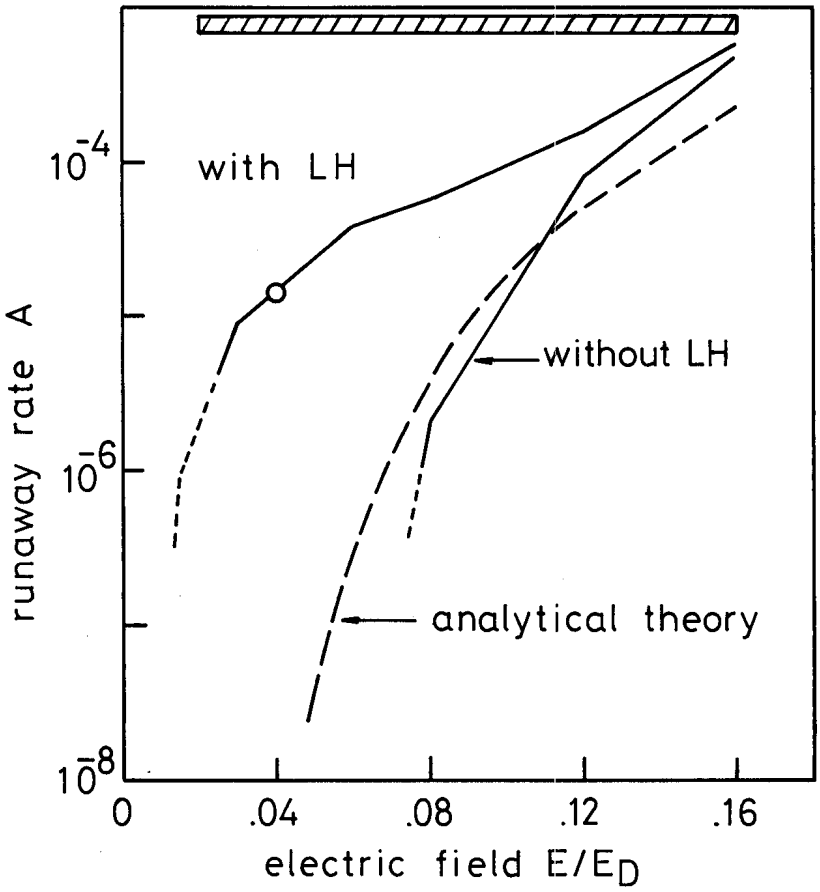
with LH
without LH
analytical theory
runaway rate A
10^{-4}
10^{-6}
10^{-8}
0
.04
.08
.12
.16
electric field E/E_D

Fig. 14

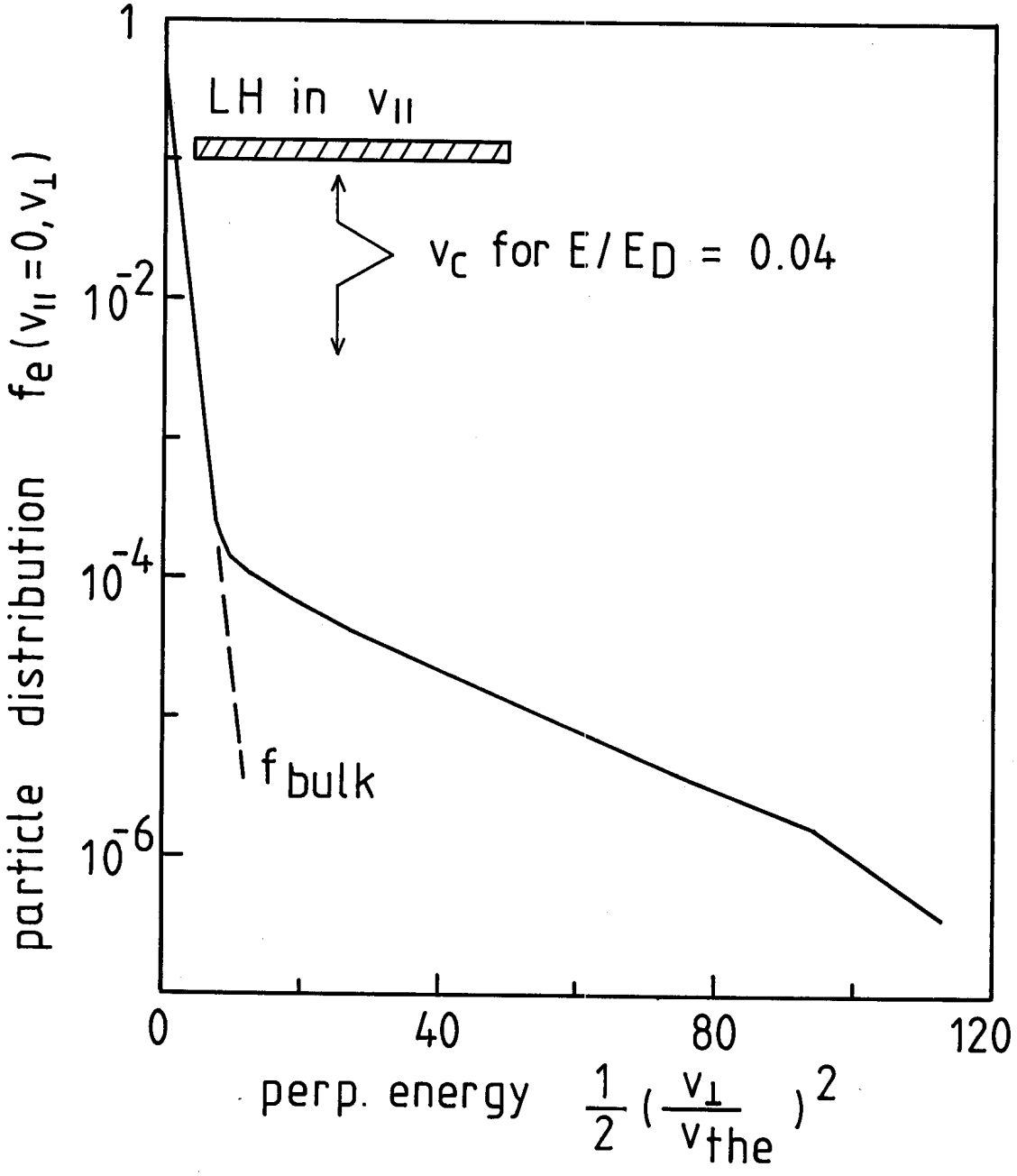
1
LH in v_{II}
v_c for $E/E_D = 0.04$
10^{-2}
10^{-4}
10^{-6}
particle distribution $f_e(v_{II}=0, v_\perp)$
f_{bulk}
0
40
80
120
perp. energy $\frac{1}{2}\left(\frac{v_\perp}{v_{the}}\right)^2$